Supplementary Information

Deconvolution of dissipative pathways for the interpretation of tapping-mode atomic force microscopy from phase-contrast

Arindam Phani[1], Ho Sang Jung[2] and Seonghwan Kim[1]
[1]Department of Mechanical and Manufacturing Engineering, University of Calgary, Calgary, AB, Canada
[2]Advanced Nano-Surface Department, Korea institute of Materials Science (KIMS), South Korea

A. Surface deformations Δa from the amplitude histogram distributions

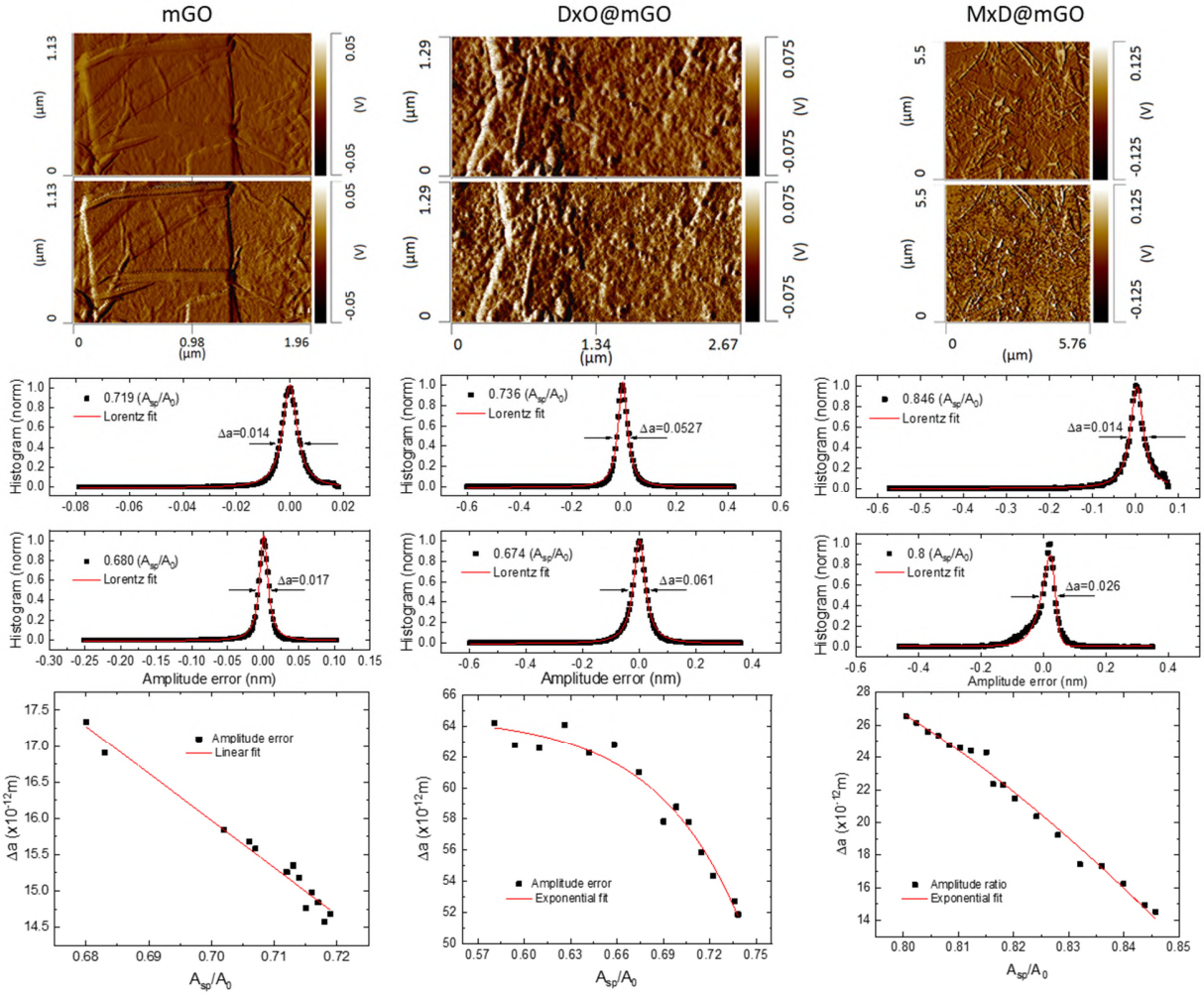

Figure S1. Surface deformations as a function of A_{sp} for mGO, DxO@mGO and MxD@mGO samples. Error bars of the deformation estimations Δa from the experimental obtained amplitude distributions are in the order of 1%. Error bars are too small to be visible at the scale of the plots. Error bars are computed as standard deviations of individual measurands, and parameters of the estimated Lorentzian fits as shown above.

B. Phase-contrast and energy dissipation results of mGO sample

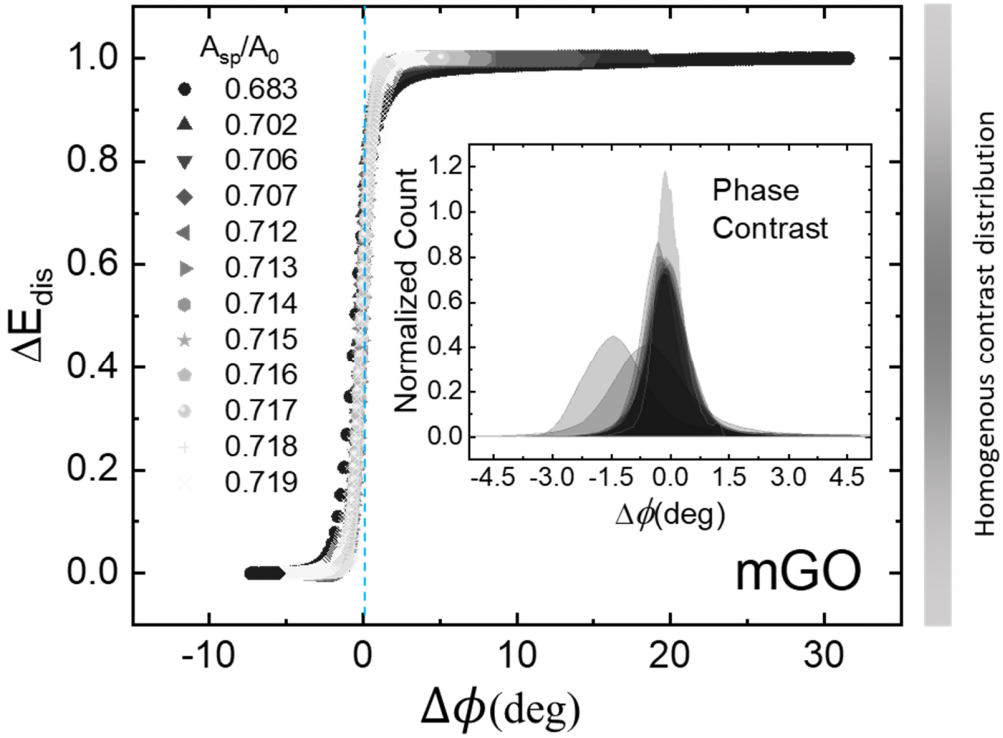

Figure S2. Phase histogram and the cumulative density graphs as a function of A_{sp} in experiments.

Clearly the phase distribution shows a predominant homogenous interaction behaviour similar to responses obtained for DxO@mGO and MxD@mGO samples at high amplitude oscillations. This is probably from the fact that mGO is expected to exhibit predominantly elastic properties at the perturbation rate of $\sim 300\ kHz$, lattice spacings being in the order of few Å only. Thus, even at low amplitude oscillations in the order of $1-2\ nm$ that could be achieved in our experimental realization, the microscopic relaxation scale remains oblivious to the underlying dynamics. The effective interaction time τ_c, though is able to follow the oscillation timescale τ_{osc}, it is still orders of magnitude slower compared to the inherent relaxation rate τ_{sur}. Thus the microscopic relaxation processes approximately appear to be in equilibrium to the tip-interface interaction energetics leading to the single stage Boltzmann-like distributions.

C. Cumulative density fit equation: Decoupling homogeneous and heterogeneous probability densities.

The normalized cumulative density function (CDF) of the phase probability histograms of experimental results can be analysed using

$$\Delta E_{dis}\left(\Delta\phi\right) = E_0 + \frac{normcdf\left(x_0, w_0, b_0\right)}{b_1\left(\frac{1}{\pi}\tan^{-1}\left(\frac{x-x_1}{w_1}\right)+\frac{1}{2}\right)} \tag{1}$$

considering coupled homogenous and heterogenous loss mechanisms at an interface. Here, $normcdf\left(x_0, w_0, b_0\right) = b_0 \int_{\phi_{\min}}^{\phi_{\max}} \frac{1}{\sqrt{2\pi}w_0} e^{-\frac{(x-x_0)^2}{2w_0^2}} dx$ is the Gaussian cumulative density with center at x_0 and homogenous linewidth of w_0 and amplitude b_0. The parameter b_0 of the fitting function is the normalized energy span of homogenous transition. The denominator $b_1\left(\frac{1}{\pi}\tan^{-1}\left(\frac{x-x_1}{w_1}\right)+\frac{1}{2}\right)$ in the fitting equation (1) represents the heterogenous or Cauchy density function with center at x_1, heterogenous linewidth of w_1 and b_1 the normalized energy span of heterogenous transition from viscous interactions. The x-axis intercepts of the curves at $\Delta\phi = 0$ provides a proportional measure of the energy conserved E_0 in the dynamics. Representative theoretical fits at different setpoint amplitudes as a function of A_{sp}/A_0 using eq (1) for both mGO and mGO+DxO are shown below. All the fits have $R^2 > 0.99$.

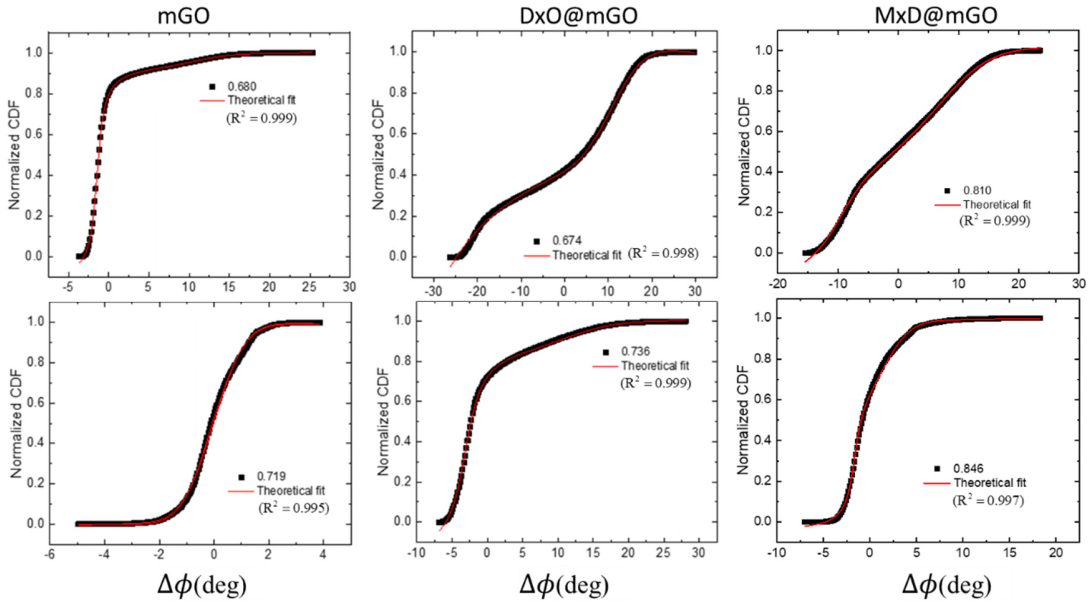

Figure S3. Representation Cumulative Density Graph and theoretical fits of at respective A_{sp}/A_0 ratios. The goodness of fit in each case are in the order of > 0.99 signifying that the regression predictions approximate the real data points to almost 100%.

A sharp contrast stemming from the relative magnitudes of homogenous and heterogeneous losses is apparent in the distributions. The physical significance of the relative scales is explained in the main article.

D. Correlation length analysis

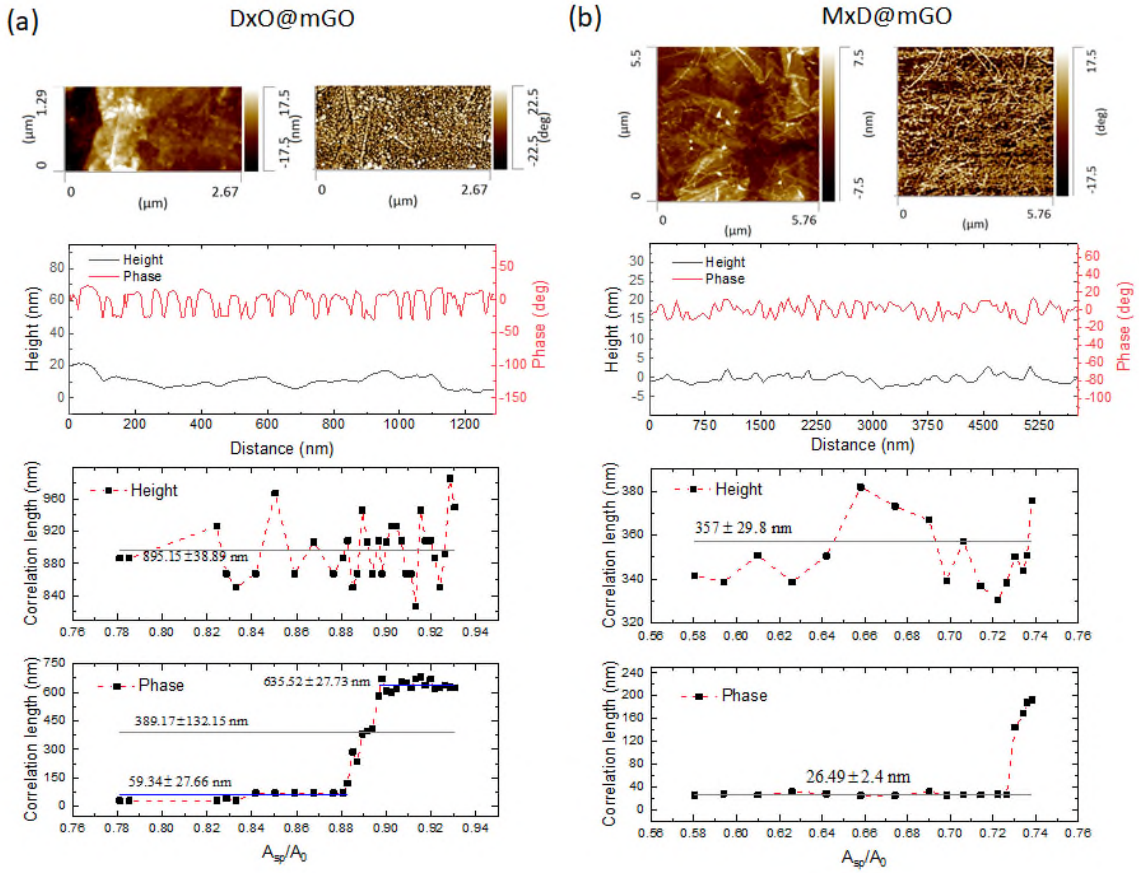

Figure S4. Correlation length analysis: The higher resolvability of heterogeneous features at ultra-light tapping is apparent. The relevance of a metastable relaxation scale argument is clear from the sigmoidal behaviour of phase correlation lengths. The error bars of the height and phase correlation length plots for each amplitude setpoint are in the order 1-2%. Error bars are computed from the standard deviations of individual measurands at each amplitude setpoint. Error estimates of mean correlation length are duly annotated in the standard notation of ± units.

Clearly the height and phase features are uncorrelated validating our argument of capturing a heterogeneous loss mechanism centered at $\Delta\phi_{-}$. The respective phase correlation length scales also show a unique multi-scale evolution behaviour as a function of A_{sp}. Unlike previous results[1] that show independence of phase correlation lengths vs A_{sp}, the sigmoidal nature highlights the importance of strain history on the measured elastic and viscous coefficients at small amplitudes. The statistical average approach of our treatment allows us to decouple the strain rate dependence from fluctuational effects as a function of the operational A_{sp} and thus in turn as a function of the tapping amplitude A. An apparent increase in phase correlation length at smaller A is suggestive of an improved resolvability of heterogeneous features, further augmenting the importance of captured additional $\Delta\phi_{-}$ transition revealing richer phase-contrast. However, the same in case of topography image remains constant within 0.1 order of standard deviation, suggesting no apparent change in height resolvability. Not to digress from the energy loss mechanism narrative, a more detailed discussion on apparent resolvability will be taken up in upcoming article to do justice on this phenomenon (that is reminiscent of velvet touch in our macro-world).

E. Tip-surface area of interaction

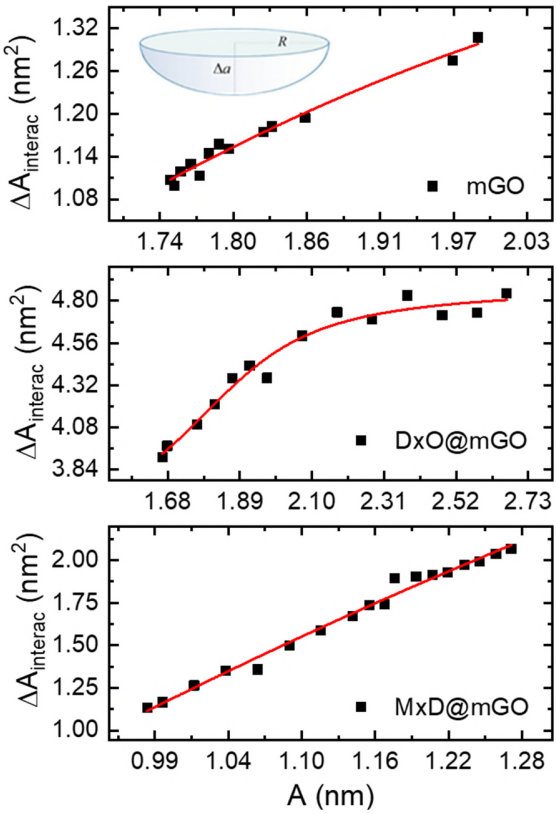

Figure S5. Effective tip-surface interaction area for mGO, DxO@mGO and MxD@mGO. The error bar estimations of interaction area are a sum of the error estimations of the deformation Δa at each amplitude setpoint and the mean tip radius, both of which are in the order of < 1%. The error bar estimations of Δa are detailed in supplementary section A. The error bars are too small to be visible at the scale of the plots.

The interaction area shows a non-linear or more specifically 2nd order polynomial dependence on the damped amplitude *A*. The relative interaction area is expected to be higher for the soft-organic molecules on account of viscous deformation as is clear from the results of DxO@mGO and MxD@mGO. The interaction area for mGO is lowest in mGO since a higher elastic property prevents deformation at the small amplitude tip forces. The trend also suggests that the interaction area for MxD would be higher compared to DxO at the same relative probing amplitude. The corresponding viscous coefficient for MxD should be higher which do corroborate to our estimations as shown in Fig 4 of the manuscript. The relative scales of the interactions area vs the probing oscillation amplitude has deeper implications on the effective strain rate amplitudes necessary to correctly decode the elastic and viscous coefficients. A more detailed study at higher amplitude resolutions would be attempted soon and results will be disclosed. In near future, re-runs with frequency tunable cantilevers made of functional materials would be attempted to generate constant strain rate data with varying frequencies and compared to existing DMA based results. The present state-of-the-art microcantilever probes limits our frequency tunability capabilities to demonstrate such an operational variation of fixed strain rate $\Delta\dot{a}$ with controlled Δa at resonance.

F. Voltage and Error calibration

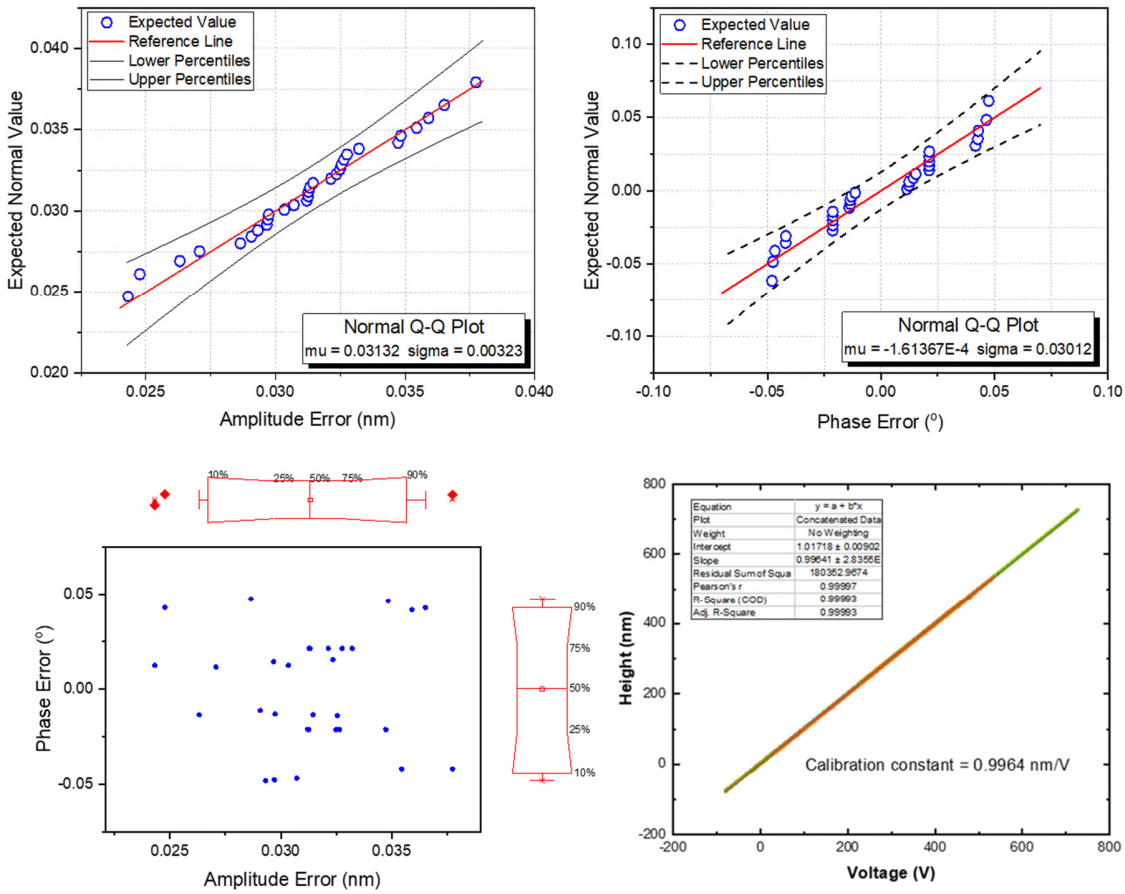

Figure S6. Phase and Amplitude error calibration Q-Q plots showing the mean and the respective standard deviations (Top left and right pane). The error in expected amplitude *A* at a selected amplitude setpoint and the corresponding phase error from expected zero phase at resonance were measured and plotted here in standard Q-Q plots. The corresponding statistical estimates of mean and standard deviation are a direct output of the statistical analysis of the measured data plotted here. Relative error values are at least one order of magnitude smaller than the measured Phase-contrast $\Delta\phi$ and oscillation amplitudes A. Bottom left pane: Shows the random nature of appearance of amplitude and phase errors. The red box-plots represent their respective quantile distributions. The very random nature of the phase and amplitude error highlights the fact that the responses are noise decorrelated facilitating correct estimates provided in the manuscript. Bottom right pane: Voltage calibration vs cantilever deflection used in amplitude and deformation estimations.

G. On the consideration of Gibbs measure and its implication in resonance dynamics

We posit that the probability $p = P(\Delta\phi_-)/P(\Delta\phi_+)$ of the random hop to transient states is expected to be described by Gibbs measure, proportional to $p = 1/Z(\beta)\cdot\exp(\beta\Delta E_{fluc})$, where β is a parameter having dimension of Energy^{-1} and $Z(\beta)$ is a normalizing constant (partition function). $Z(\beta)$ is taken to be a slower varying function of β compared to the exponent. The choice of Gibbs measure is appropriate here, as it is

known to apply to a statistical ensemble of weak interactions near equilibrium as in our case of adiabatic crossover. Moreover, the applicability of Gibbs measure has been proven to systems under very general assumptions[2]. It is thus appropriate to choose $1/\beta$, having the dimension of energy, to be $1/\beta = b\Delta E_{osc}$ with b a constant. In our case b is fitting exponential coefficient in the order of 10^1.

H. AFM-IR results of mGO

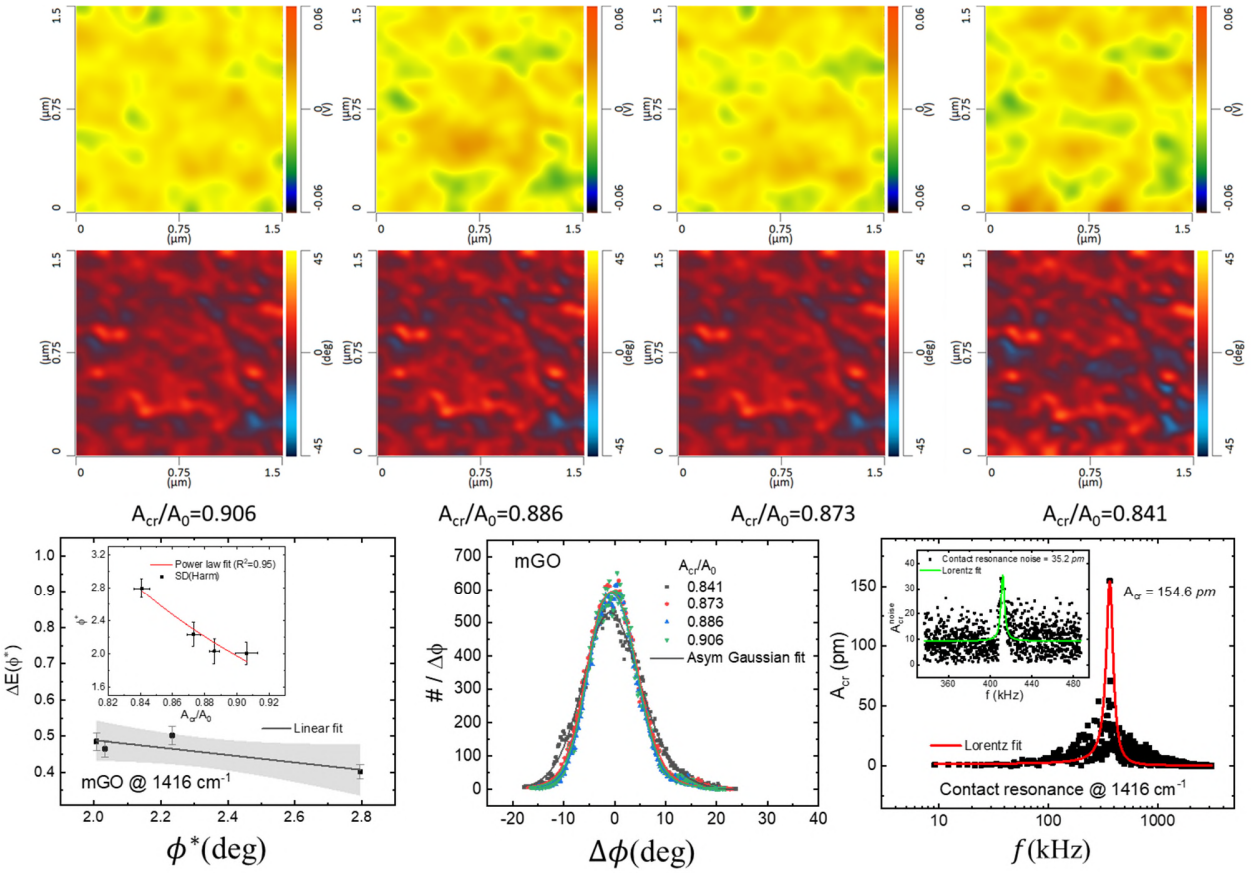

Figure S7. Observed IR-contrast and phase-contrast as a function of contact resonance amplitudes A_{cr} that is in the order of $35.2\ pm$. Bottom left pane: Explains the ratio of the heterogenous to homogenous energy losses vs the apparent phase contrast as derived from the phase histograms (Bottom middle pane) using the theoretical considerations in manuscript. Phase-contrast essentially originates from the contact resonance noise as shown in bottom right pane inset. On the contrary phase-contrast as observed in the case of DxO and MxD at 1416 cm^{-1} and 1455 cm^{-1}, respectively, originate from contact enhanced resonance amplitude that is the order of $154.6\ pm$ ensuring oscillations in the crossover regime as described in the manuscript. Fluctuational transitions dominate in this pseudo tapping mode operational regime which has been discussed in detail in the manuscript.

I. Comparison of results obtained in the case of DxO@Si

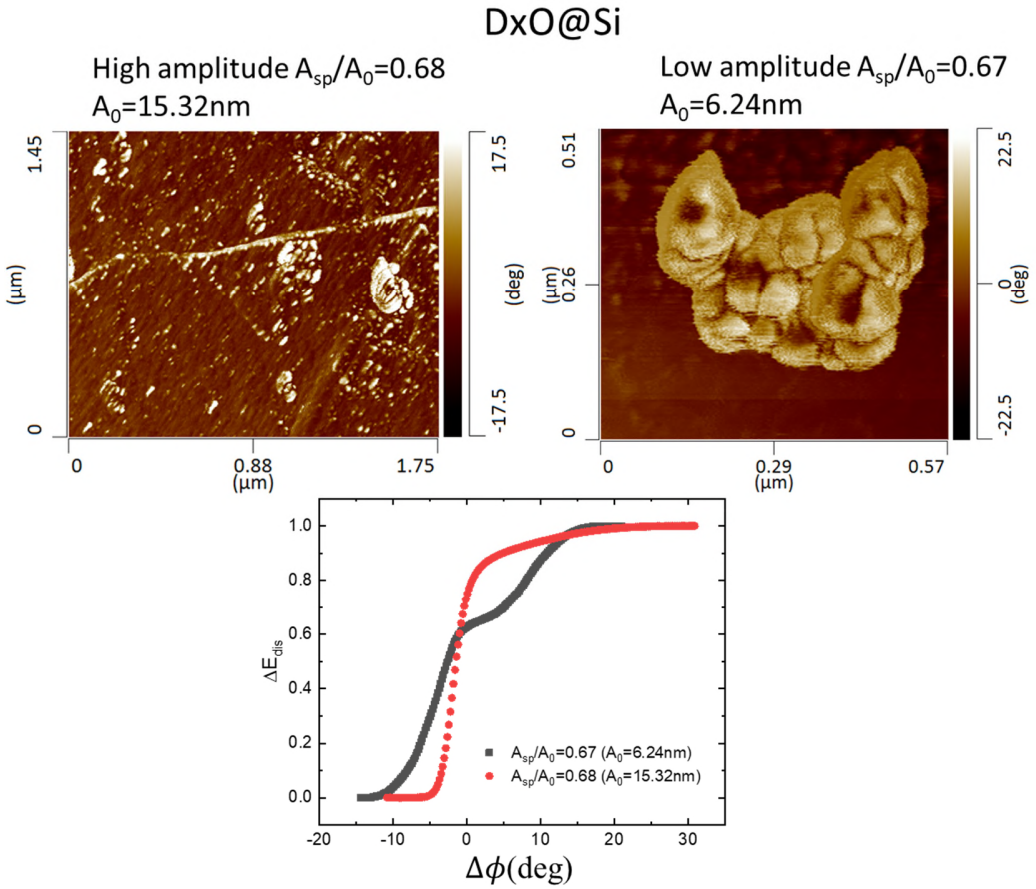

Figure S8. Phase images and their cumulative density graphs at high and low amplitude tapping obtained in the case of DxO crystallized on a bare Si surface.

The appearance of the heterogenous loss stage is evident in the case of low amplitude tapping in the form of a two-stage phase distribution (black squares). The phase distribution obtained for high amplitude tapping follows a single stage homogenous Boltzmann-like distribution signifying homogenous loss process only. This comparative representative data for DxO on Si asserts to our arguments made in the manuscript. A more detailed study on drug clusters on Si will be taken up later.

J. Frequency responses and determined spring constants using Sader model [2]

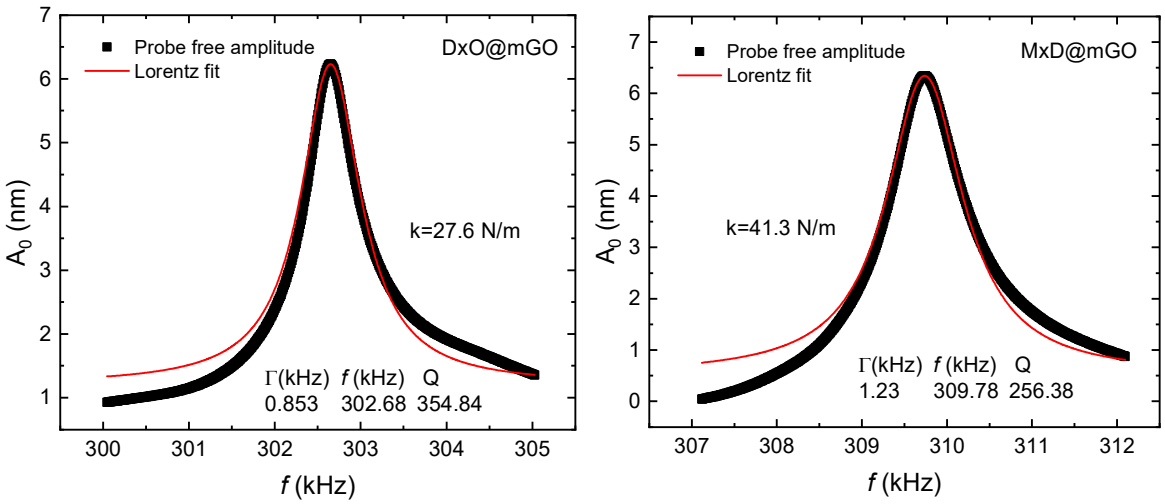

Figure S9. Frequency response characteristics of tapping mode AFM cantilevers used in imaging mGO and DxO@mGO is shown in the left pane. The same for imaging MxD@mGO is shown on the right pane. The spring constants determined using Sader's model[3] give values of k = 27.6 N/m and 41.3 N/m, respectively, as shown. These values are employed in determining the surface energy and viscous coefficient calculations in main text.

Supplementary References

1. Liu, Y. H. *et al.* Characterization of nanoscale mechanical heterogeneity in a metallic glass by dynamic force microscopy. *Phys. Rev. Lett.* **106**, 125504 (2011).

2. Landau, L. D. & Lifshitz, E. M. *Statistical Physics*. *Statistical Physics* (Butterworth-Heinemann, 1980). doi:10.1142/3526

3. http://www.ampc.ms.unimelb.edu.au/afm/calibration.html